舶用 디이젤機關軸系 세로 비틀림 連成 自由振動의 理論的 解析

全 孝 重

槪 要

最近 船舶의 高速化. 大形化에 따라서 크랑크軸系의 振動問題가 또다시 重要한 位置를 차지하게 되었으며, 特히 세로(縱) 振動 및 세로비틀림連成振動이 問題의 焦點이다.

前者에 對하여서는 이미 많은 論文이 發表되었으나, 비틀림 振動의 경우와 같이 信賴할 수 있는 方法은 아즉 밝혀지지 않고 있다. 또한 後者에 對하여서는 그 發生機構 조차도 밝혀지지 않았으며 스케일모델實驗에 의한 方法이 提案되고 있을 程度이다.

이 論文에서는 (1) 새로운 모델系를 設定하여 세로 振動, 비틀림振動 및 2 種類의 가로(橫)振動을 表示할 수 있도록 하였으며, (2) 各部의 용수철係數를 設計圖面으로 부터 直接 理論的으로 求할 수 있는 方法을 提案하고, (3) 마트릿그스 法을 導入하여 連成振動方程式을 쓰고, 이것을 固有値問題로 變換하여 야코비 回轉法에 의하여 電子計算機로 푸는 方法을 說明한다. (4) 解는 한꺼번에 軸系全體의 自由振動數(固有値) 및 모—드(固有벡터)를 주며 이들 중에 세로 비틀림 連成振動도 包含된다.

이 方法을 構造가 全혀 다른 3個의 實際機關에 適用하여 實測値와 比較하여 본 結果, 良好한 一致를 보였다. 또한 이들을 從來의 方法에 의한 비틀림 및 세로 振動의 計算値와 比較하고, 그외에 系의 數値變更效果를 吟味하였다.

最後로 이 方法은 홀싸—法 보다도 電子計算에 便利하다는 것, 卽 從來의 非連成 비틀림 혹은 非連成 세로振動의 計算에도 利用할 수 있음을 밝혔다.

Theoretical Analysis of the Coupled Torsional-axial Undamped Vibration of the Marine Diesel Engine Shafting

By

Hiojung Jeon

Abstract

Ever growing engine size and power have renewed such crankshaft trouble as axial or coupled torsional-axial vibration. For the former mode some empirical methods have been proposed to calculate its natural frequencies, but are not so reliable as ones for torsional vibration. For the latter it seems to have been dealt with nothing but an experimental, scale-model method.

In this paper, (1) a new equivalent system of crankshaft is supposed so as to tolerate 4 degrees of

This work was performed under the guidance of Pro. Dr. K. Tsuda at University of Tokyo.

freedom : axial, torsional and two kinds of lateral vibration. (2) Theoretical, not empirical equations for calculating stiffness values of the shafting are derived, so that a design-stage forcast of the modes of shaft vibration is possible. (3) Equations of motion are written in matrices, transformed into eigen-value problems and solved with the Jacobi-rotation method on a digital computer, not iteratively but directly. (4) The solution gives every mode and frequency on one chart, including coupled torsional axial modes which have never been correctly explained before.

Three kinds of shafting were investigated, and their solutions showed fairly good agreements with the measured data on board, The author recommends to apply this new matrix method not only to coupled system as above, but also to simple system without coupling—pure torsional or pure axial—in place of Holzer method for convenience in digital computation.

1. Introduction

In recent years, the development of the marine Diesel engine toward more and more powerful and also increasingly larger units has brought about shaft troubles due to axial or coupled torsional-axial vibration. [15] For the former some empirical methods to calculate natural frequencies and modes have been proposed, but they are not so reliable as ones for the torsional vibration. For the latter it seems to have been dealt with nothing but an experimental, scale-model method. [11]

This paper presents a theoretical method to solve crankshaft vibration problem without isolation of four modes from one another: torsional vibration, axial vibration and two kinds of lateral vibration, introducing an original equivalent system with many degrees of freedom and applying a matrix technique combined with digital computation.

Further, the author's method more conveniently applies to isolated torsional vibration problems than the old iterative method, which is yet popular even at digital computation in spite of the recent remarkable progress of computing techniques and equipments.

2. Method of analysis

2.1 Equation of motion

Fig. 1 shows the original reduction of an eight cylinder crank shafting. The center line of the shaft from fore-end to rear is defined to be x axis, with its origin at the middle point of the fore-end journal bearing. Axes y and z rotate around x with the mean speed of the shaft, where y-axis is put parallel to the mean figure of the fore-end crank arm center line. The positive directions of forces and moments correspond to that of co-ordinate axes. The equivalent system has for every crank journal one inertia body with four degrees of freedom: x-motion, θ-motion around x, φ around y, and ψ around z, corresponding to axial, torsional, lateral and another lateral vibration respectively. The mass moment of inertia of the i^{th} body, I_{xi}, amounts to the sum of inertia moments on both sides of the journal, including reciprocating masses, i. e. the sum of the halves of the inertia moments derived at conventional torsional vibration analysis. The mass of the i^{th} body, M_i, however, excludes reciprocating masses. Finally, moments of inertia around the other axes are defined as

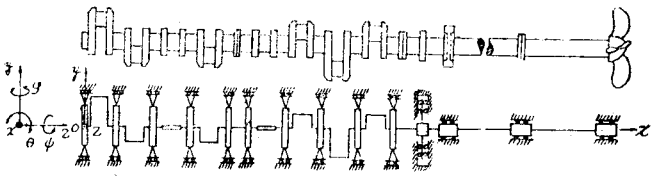

Fig. 1 The equivalent model of an 8-cylinder crank shafting

$$I_{yi}=I_{zi}=\frac{1}{2}I_{xi}$$

The definition of shaft stiffness between inertia bodies is as follows, although its theoretical derivation will be described in Section 3. Consider two bodies adjacent each other, the i-1th and the ith body, and name their centers of gravity Point i-1 and Pt. i respectively. Fix Pt. i and give Pt. i-1 a unit displacement in x-direction. Then the induced force at Pt. i should be equal to k_{xixi-1} multiplied by a unit length, i. e. k represents stiffness. For another example, fix Pt. i and give Pt. i-1 a unit ψ-displacement. Then, the induced moment in θ-direction at Pt. i-1 is $k_{\theta i-1\psi i-1}$. The followings define the abbreviation of those suffix expressions, in case of Pt. i fixed and Pt. i-1 given a unit displacement in x-, θ-, φ-, ψ-direction.

$k_{xi-1xi-1}=k_{11}$, $k_{\theta i-1xi-1}=k_{21}$, $\cdots\cdots k_{\psi i-1xi-1}=k_{41}$,
$k_{xixi-1}=k_{51}$, $\cdots\cdots$, $k_{\psi ixi-1}=k_{81}$
$k_{xi-1\theta i-1}=k_{12}$, $k_{\theta i-1\theta i-1}=k_{22}$, $\cdots k_{\psi i-1\theta i-1}=k_{42}$,
$k_{xi\theta i-1}=k_{52}$, $\cdots$, $k_{\psi i\theta i-1}k_{82}$
$k_{xi-1\varphi i-1}=k_{13}$, $k_{\theta i-1\varphi i-1}=k_{23}$, $\cdots k_{\psi i-1\varphi i-1}=k_{43}$,
$k_{xi\varphi i-1}=k_{53}$, $\cdots$, $k_{\psi i\varphi i-1}=k_{83}$
$k_{xi-1\psi i-1}=k_{14}$, $k_{\theta i-1\psi i-1}=k_{24}$, $\cdots k_{\psi i-1\psi i-1}=k_{44}$,
$k_{xi\psi i-1}=k_{54}$, $\cdots$, $k_{\psi i\psi i-1}=k_{84}$

Now, fix Pt. i-1 and give Pt. i a unit displacement. In this case, the abbreviation of k-expressions is defined as

$k_{xi-1xi}=k_{15}$, $k_{\theta i-1xi}=k_{25}$, $\cdots k_{xixi}=k_{55}$, $k_{\theta ixi}=k_{65}$,
$\cdots k_{\psi ixi}=k_{85}$
$k_{xi-1\theta i}=k_{16}$, $k_{\theta i-1\theta i}=k_{26}$, $\cdots k_{xi\theta i}=k_{56}$,
$k_{\theta i\theta i}=k_{66}$, $\cdots k_{\psi i\theta i}=k_{86}$
$k_{xi-1\varphi i}=_{17}$, $k_{\theta i-1\varphi i}=_{27}$, $\cdots k_{xi\varphi i}=k_{57}$,
$k_{\theta i\varphi i}=k_{67}$, $\cdots k_{\psi i\varphi i}=k_{87}$
$k_{xi-1\psi i}=k_{18}$, $k_{\theta i-1\psi i}=_{28}$, $\cdots k_{xi\psi i}=k_{58}$,
$k_{\theta i\psi i}=k_{68}$, $\cdots k_{\psi i\psi i}=k_{88}$

The same idea applies to the combination of the ith and the i+1th body:

$k_{xixi}=\bar{k}_{11}$, $k_{\theta ixi}=\bar{k}_{21}$, $\cdots k_{xi+1xi}=k_{51}$,
$k_{\theta i+1xi}=\bar{k}_{61}$, $\cdots k_{\psi i+1xi}=\bar{k}_{81}$
$k_{xi\theta i}=\bar{k}_{12}$, $k_{\theta i\theta i}=\bar{k}_{22}$, $\cdots k_{xi+1\theta i}=k_{52}$, $k_{\theta i+1\theta i}=\bar{k}_{62}$,
$\cdots k_{\psi i+1\theta i}=\bar{k}_{82}$
$k_{xi\varphi i}=\bar{k}_{13}$, $k_{\theta i\varphi i}=\bar{k}_{23}$, $\cdots k_{xi+1\varphi i}=k_{63}$, $k_{\theta i+1\varphi i}=\bar{k}_{63}$,
$\cdots k_{\psi i+1\varphi i}=\bar{k}_{83}$
$k_{xi\psi i}=\bar{k}_{14}$, $k_{\theta i\psi i}=\bar{k}_{24}$, $\cdots k_{xi+1\psi i}=\bar{k}_{54}$, $k_{\theta i+1\psi i}=\bar{k}_{64}$,
$\cdots k_{\psi i+1\psi i}=\bar{k}_{84}$
$k_{xixi+1}=\bar{k}_{15}$, $k_{\theta ixi+1}=\bar{k}_{25}$, $\cdots k_{xi+1xi+1}=\bar{k}_{55}$,
$k_{\theta i+1xi+1}=\bar{k}_{65}$, $\cdots k_{\psi i+1xi+1}=\bar{k}_{85}$
$k_{xi\theta i+1}=\bar{k}_{16}$, $k_{\theta i\theta i+1}=\bar{k}_{26}$, $\cdots k_{xi+1\theta i+1}=\bar{k}_{56}$,
$k_{\theta i+1\theta i+1}=\bar{k}_{66}$, $\cdots k_{\psi i+1\theta i+1}=_{86}$
$k_{xi\varphi i+1}=\bar{k}_{17}$, $k_{\theta i\varphi i+1}=\bar{k}_{27}$, $\cdots k_{xi+1\varphi i+1}=_{57}$,
$k_{\theta i+1\varphi i+1}=\bar{k}_{67}$, $\cdots k_{\psi i+1\varphi i+1}=\bar{k}_{87}$
$k_{xi\psi i+1}=\bar{k}_{18}$, $k_{\theta i\psi i+1}=\bar{k}_{28}$, $\cdots k_{xi+1\psi i+1}\bar{k}_{58}$,
$k_{\theta i+1\psi i+1}=\bar{k}_{68}$, $\cdots k_{\psi i+1\psi i+1}=\bar{k}_{88}$

Among those shown above, expressions k_{11}, k_{12}, $\cdots k_{15}$, $\cdots$ k_{18}, $\bar{k}_{11}$, $\bar{k}_{12}$, $\cdots$ $\bar{k}_{15}$, $\cdots$ $\bar{k}_{18}$, are used common without any regard to body number for the sake of simplicity, in spite of any possible confusion. Using the k-expressions except those which are definitely zero equations of undamped motion of an n-cylinder engine shafting are written as follows. In the first equation of the n+2th body, k_o represents the thrust block stiffness, although the thrust block should be numbered n+3 in case it is at a distance from the rear-end throw.

$$\left.\begin{aligned} &M_1\ddot{x}_1+k_{11}x_1+k_{14}\psi_1+k_{15}x_2+k_{18}\psi_2=0 \\ &I_{x1}\ddot{\theta}_1+k_{22}\theta_1+k_{23}\varphi_1+k_{26}\theta_2+k_{27}\varphi_2=0 \end{aligned}\right]$$

$$I_{y1}\ddot{\varphi}_1+k_{32}\theta_1+k_{33}\varphi_1+k_{36}\theta_2+k_{37}\varphi_2=0$$
$$I_{z1}\ddot{\psi}_1+k_{41}x_1+k_{44}\psi_1+k_{45}x_2+k_{48}\psi_2=0$$
……the 1st inertia body

$$M_2\ddot{x}_2+k_{51}x_1+k_{54}\psi_1+(k_{55}+\bar{k}_{11})x_2+\bar{k}_{15}\varphi_2+(k_{58}+\bar{k}_{14})\psi_2+\bar{k}_{15}x_3+\bar{k}_{17}\varphi_3+\bar{k}_{18}\psi_3=0$$
$$I_{x2}\ddot{\theta}_2+k_{26}\theta_1+k_{63}\varphi_1+(k_{66}+\bar{k}_{22})\theta_2+(k_{67}+\bar{k}_{23})\varphi_2+\bar{k}_{24}\psi_2+\bar{k}_{26}\theta_3+\bar{k}_{27}\varphi_3+\bar{k}_{28}\psi_3=0$$
$$I_{y2}\ddot{\varphi}_2+k_{72}\theta_1+k_{73}\varphi_1+\bar{k}_{31}x_2+(k_{76}+\bar{k}_{32})\theta_2+(k_{77}+\bar{k}_{33})\varphi_2+\bar{k}_{34}\psi_2+\bar{k}_{35}x_3+\bar{k}_{36}x_3+\bar{k}_{36}\theta_3+\bar{k}_{37}\varphi_3+\bar{k}_{38}\psi_3=0$$
$$I_{z2}\ddot{\psi}_2+k_{81}x_1+k_{84}\psi_1+(k_{85}+\bar{k}_{41})x_2+\bar{k}_{42}\theta_2+\bar{k}_{43}\varphi_2+(k_{88}+\bar{k}_{44})\psi_2+\bar{k}_{45}x_3+\bar{k}_{46}\theta_3+\bar{k}_{47}\varphi_3+\bar{k}_{48}\psi_3=0$$
…… the 2nd inertia body

……

$$M_i\ddot{x}_i+k_{51}x_{i-1}+k_{53}\varphi_{i-1}+k_{54}\psi_{i-1}+(k_{55}+\bar{k}_{11})x_i+(k_{57}+\bar{k}_{13})\varphi_i+(k_{58}+\bar{k}_{14})\psi_i+\bar{k}_{15}x_{i+1}+\bar{k}_{17}\varphi_{i+1}+k_{18}\psi_{i+1}=0$$
$$I_{xi}\ddot{\theta}_i+k_{62}\theta_{i-1}+k_{63}\varphi_{i-1}+k_{64}\psi_{i-1}+(k_{66}+\bar{k}_{22})\theta_i+(k_{67}+\bar{k}_{23})\varphi_i+(k_{68}+\bar{k}_{24})\psi_i+\bar{k}_{26}\theta_{i+1}+\bar{k}_{27}\varphi_{i+1}+k_{28}\psi_{i+1}=0$$
$$I_{yi}\ddot{\varphi}_i+k_{71}x_{i-1}+k_{72}\theta_{i-1}+k_{73}\varphi_{i-1}+k_{74}\psi_{i-1}+(k_{75}+\bar{k}_{31})x_i+(k_{76}+\bar{k}_{32})\theta_i+(k_{77}+\bar{k}_{33})\varphi_i+(k_{78}+\bar{k}_{34})\psi_i+\bar{k}_{35}x_{i+1}+\bar{k}_{36}\theta_{i+1}+\bar{k}_{37}\varphi_{i+1}+\bar{k}_{38}\psi_{i+1}=0$$
$$I_{zi}\ddot{\psi}_i+k_{81}x_{i-1}+k_{82}\theta_{i-1}+k_{83}\varphi_{i-1}+k_{84}\psi_{i-1}+(k_{85}+\bar{k}_{41})x_i+(k_{86}+\bar{k}_{42})\theta_i+(k_{87}+\bar{k}_{34})\varphi_i+(k_{88}+\bar{k}_{44})\psi_i+\bar{k}_{45}x_{i+1}+\bar{k}_{46}\theta_{i+1}+\bar{k}_{47}\varphi_{i+1}+\bar{k}_{48}\psi_{i+1}=0$$
……the i^{th} inertia body

……

$$M_{n+1}\ddot{x}_{n+1}+k_{51}x_n+k_{53}\varphi_n+k_{54}\psi_n+(k_{55}+\bar{k}_{11})x_{n+1}+k_{57}\varphi_{n+1}+k_{58}\psi_{n+1}+\bar{k}_{15}x_{n+2}=0$$
$$I_{xn+1}\ddot{\theta}_{n+1}+k_{62}\theta_n+k_{63}\varphi_n+k_{64}\psi_n+(k_{66}+\bar{k}_{22})\theta_{n+1}+k_{67}\varphi_{n+1}+k_{68}\psi_{n+1}+\bar{k}_{26}\theta_{n+2}=0$$
$$I_{yn+1}\ddot{\varphi}_{n+1}+k_{71}x_n+k_{72}\theta_n+k_{73}\varphi_n+k_{74}\psi_n+k_{75}x_{n+1}+k_{76}\theta_{n+1}+(k_{77}+\bar{k}_{33})\varphi_{n+1}+k_{78}\psi_{n+1}=0$$
$$I_{zn+1}\ddot{\psi}_{n+1}+k_{81}x_n+k_{82}\theta_n+k_{83}\varphi_n+k_{84}\psi_n+k_{85}x_{n+1}+k_{86}\theta_{n+1}+k_{87}\varphi_{n+1}+(k_{88}+\bar{k}_{44})\psi_{n+1}=0$$
……the n+1th inertia body

$$M_{n+2}\ddot{x}_{n+2}+k_{51}x_{n+1}+(k_{55}+\bar{k}_{11}+k_o)x_{n+2}+\bar{k}_{15}x_{n+3}=0$$
$$I_{xn+2}\ddot{\theta}_{n+2}+k_{62}\theta_{n+1}+(k_{66}+\bar{k}_{22})\theta_{n+2}+\bar{k}_{26}\theta_{n+3}=0$$
…the n+2th inertia body—thrust bearing

……

$$M_p\ddot{x}_p+\bar{k}_{51}x_{p-1}+\bar{k}_{55}x_p=0$$
$$I_{xp}\ddot{\theta}_p+\bar{k}_{62}\theta_{p-1}+\bar{k}_{66}\theta_p=0$$
…the rear-end inertia body—propeller ……(1)

2.2 Method of solution.

The complicated appearance of Eqs. (1) vanishes by introducing matrix expression as

$$[M]\{\ddot{x}\}+[K]\{x\}=0 \quad \cdots\cdots(2)$$

where $[M]$, $[K]$ denote inertia moment matrix abbreviated as mass matrix and stiffness matrix respectively, and $\{x\}$ is coloumn vector or coloumn matrix of co-ordinates and $\{\ddot{x}\}$ represents the one of the second derivatives of x.

Let $[K]^{-1}=[F]$, then

$$[F][M]\{\ddot{x}\}+\{x\}=0 \quad \cdots\cdots(3)$$

where $[F]$ is flexibility matrix, which consists of influence numbers. Assume the solution of Eq. (2) to be

$$\{x\}=\{a\}e^{\pm jwt} \quad \cdots\cdots(4)$$

where $\{a\}$ is amplitude matrix.

From Eq. (2) and (4)

$$(-\omega^2[M]+[K])\{a\}=0 \quad \cdots\cdots(5)$$

The standard deduction process (see references 17, 18 or 20 for details) changes Eq. (5) into the following determinant:

$$|[K]-[M]|=0 \quad \cdots\cdots(6)$$

which leads to characteristic equation of eigenvalues, ω^2.

For the solution of eigenvalue problems there are two methods. The first method expands Eq. (6) with respect to ω^2 into a polynomial, then solves it. However, this method is practically impossible even by digital computation, because of as many degrees of freedom as 50.

The second method [16] [17] [18] [19] [20] may be subdivided into several, two of which will be described. Transform Eq. (5) into.

$$[M]^{-1}[K]\ \{a\}=\omega^2\{a\} \quad \cdots\cdots(7)$$

Solve this equation digitally, computing for ω^2 and $\{a\}$ by matrix iteration process, which is much more economical than solving an n^{th} order polynomial. Although this method has been sometimes manually applied to obtain a few largest eigenvalues and corresponding eigenvectors, in this case smallest eigenvalues are required, so that Eq. (7) is rewritten as

$$[K]^{-1}[M]\{a\}=\frac{1}{\omega^2}\{a\} \quad \cdots\cdots(8)$$

But, this expression necessitates derivation of flexibility matrix $[F]=[K]^{-1}$, besides accuracy of higher order solutions is not sufficient. Furthermore, if determinant $|K|$ or $|M|$ is singular, its null elements should be taken away, making a reduction of matrix order by the degree of singularity. Unfortunately, crankshaft has a singularity at $\omega=0$ where $|K|=0$, since it allows movement as a rigid body. In addition, eigenvalues equal or nearly equal to each other or one another also make trouble.

The second subdivision named Jacobi rotation method yields ω and $\{a\}$ without sacrificing accuracy and time. Transform Eq. (5) into

$$\frac{1}{\omega^2}[M]^{\frac{1}{2}}\{a\}=[M]^{\frac{1}{2}}[K]^{-1}[M]^{\frac{1}{2}}[M]^{\frac{1}{2}}\{a\} \quad \cdots\cdots(9)$$

Once more, transform Eq. (9) into a simpler form as

$$\omega^2\{\theta\}=[B]\{\theta\} \quad \cdots\cdots(10)$$

where

$$\{\theta\}=[M]^{\frac{1}{2}}\{a\}$$

$$[B]=[M]^{-\frac{1}{2}}[K][M]^{-\frac{1}{2}}$$

Application of Jacobi rotation to Eq. (10) gives ω^2 and $\{\theta\}$, then from them ω and $\{a\}$. This method is a diagonalization process, which means transformation of determinant without any change of eigenvalues into such determinant that all the elements other than those on the principal diagonal are zero, so as to easily obtain eigenvalues. However, only a real symmetric matrix applies to this method and fortunately the equivalent system shown in Fig. 1 gives such a matrix. In addition, this process has no trouble, even in case of equal eigenvalues or at singular points.

In conclusion, the author chooses the Jacobi rotation method.

3. Stiffness expressions

3.1 Thrust block stiffness

Since theoretical estimation of the thrust block stiffness is yet impossible, it must be measured directly or indirectly. When the thrust block is apart from the engine, direct measurement is possible. If it is built in the engine, or its housing is bolted to the engine block, its stiffness is possibly deduced from the running test results. The author presents a method of deduction as follows.

In case of nodeless (1st mode) axial vibr-

ation, the resultant inertia force of shafting loads the thrust block as

$$\sum_{i=1}^{p} m_i \ddot{x}_i + k_0 x_{n+2} = 0 \cdots\cdots (11)$$

Let $x_i = \bar{x}_i \sin\omega_0 t$ and $\omega_0^2 = \lambda_0$ Then

$$\sum_{i=1}^{p} m_i \bar{x}_i \lambda_0 = \bar{x}_{n+2} k_0 \cdots\cdots (11)$$

and $$k_0 = \left(\frac{\bar{x}_1}{\bar{x}_{n+2}}\right) \sum_{i=1}^{p} m_i \left(\frac{\bar{x}_i}{\bar{x}_1}\right) \lambda_0 \cdots\cdots (12)$$

where λ_0 is obtained at the running test, and $(\bar{x}_i/\bar{x}_1)$ values are obtainable by application of Holzer method to the shafting. Practically however, this application should be done in three processes: the first deals with $\bar{x}_i/\bar{x}_1$ from fore-end inertia upto thrust block, and the second $\bar{x}_i/x_p$ from propeller upto thrust block, and the final puts the fore side calculation of x_{n+2} equal to the rear-calculated x_{n+2}.

Or, if the above process appears complicated, one may get a rough answer from the following relation, assuming a simplified equivalent system in Fig. 2.

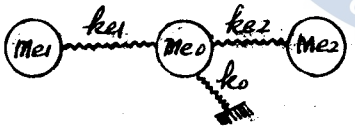

Fig. 2 The simplified equivalent system of the marine Diesel engine shsfting

$$k_0 = \lambda_0 m_{e0} + \frac{k_{e1}^2}{k_{e1} - \lambda_0 m_{e1}} + \frac{k_{e2}^2}{k_{e2} - \lambda_0 m_{e2}} - (k_{e1} + k_{e2}) \cdots\cdots (13)$$

where m_{e1}, m_{e0}, m_{e2} correspond to crank throws, thrust block and propeller respectively and k_{e1}, k_{e2} are stiffnesses between them.

3.2 Influence numbers of a unit crank throw.

Consider a single crank throw, and define its axis of rotation from fore-end to rear to be X-axis, with its origin at the middle point of the fore journal, combined with Y-and Z-axis, which are parallel and perpendicular to the crank arm respectively. As to angular displacements around these axes, Θ, Φ, Ψ correspond to X, Y, Z. The followings give influence numbers of this throw under various end loadings.

3.2.1 Influence numbers under loading in X-direction.

As shown in Fig. 3, fix B-end and put a unit force $Fx = 1$ onto the simply supported end, A. Since influence numbers, in this case, are X-, Θ-, Φ- and Ψ- displacements divided by Fx, the deformation of this indeterminate structure should be solved. At first the indeterminate fixing moment at B, α, is derived, supposing B-end simply supported, as a moment that cancels out the Ψ-displacement at B due to $Fx = 1$, Ψ_B. Such elastic deformation is easily obtained by application of Castigliano's theorem, which generally gives enough accuracy in spite of neglecting strain energy caused by stresses other than bending and twisting. [19]

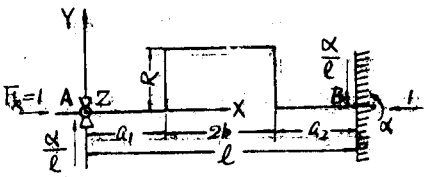

Fig. 3 Force and moment induced by the loading in X-axis

Thus,

$$\Psi_B = \frac{-2Rb(a_1+b)}{lEJ_2} + \frac{-R^2(a_1+b)}{lEJ_z} \cdots (14)$$

where E is Young's modulus, and J_1, J_2, J_z denote moments of inertia of sectional area around Z-axis corresponding to crank pin, journal and arm respectively.

Angular displacement due to a unit moment at B-end around Z-axis is

$$\Psi'_B = \frac{a_1^3+l^3-(a_1+2b)^3}{3EJ_1l^2}+\frac{(a_1+2b)^3-a_1^3}{3EJ_2l^2}+\frac{R\{a_1^2+(l-a_2)^2\}}{l^2EJ_z} \quad \cdots\cdots(15)$$

From (14), (15) and $F_X\Psi_B+\alpha\Psi'_B=0$

$$\alpha=\frac{\frac{2Rb(a_1+b)}{lEJ_2}+\frac{R^2(a_1+b)}{lEJ_x}}{\frac{a_1^3+l^3-(a_1+2b)^3}{3EJ_1l^2}+\frac{(a_1+2b)^3-a_1^3}{3EJ_2l^2}+\frac{R\{a_1^2+(l-a_2)^2\}}{EJ_zl^2}}$$

Then X-displacement of A-end, X_A is derived and leads to the expression of the influence number in X-direction due to X-forces, $f_{XX}=X_A/F_X$, i.e.,

$$f_{XX}=\frac{1}{EJ_1l^2}\left[\left(\frac{\alpha^2a_1^3}{3}\right)+\left(\frac{\alpha^2a_2}{3}\right)\{l^2+l(a_1+2b)+(a_1+2b)^2\}\right]+\frac{2b}{EJ_2l^2}\left\{(lR)^2-2lR\alpha(a_1+b)+\frac{\alpha^2}{3}(3a_1^2+6a_1b+4b^2)\right\}+\frac{R}{EJ_xl^2}\left[\frac{2}{3}l^2R^2-lR\alpha(l+a_1-a_2)+\alpha^2\{a_1^2+(l-a_2)^2\}\right] \quad \cdots\cdots(17)$$

Since Θ- or Φ-displacement of A-end does not occur

$$f_{\Theta X}=0 \quad \cdots\cdots(18)$$

$$f_{\Phi X}=0 \quad \cdots\cdots(19)$$

Further, the relation $f_{ij}=f_{ji}$ holds for any i and j as the result of Maxwell—Betti's reciprocal theorem.

In case $J_1=J_2=J$ and $a_1=a_2=a$, Eqs. (16) and (17) are simplified as

$$\alpha=\frac{\frac{2}{R}\left(\frac{2b}{J}+\frac{R}{J_x}\right)}{\frac{l}{3J}+\frac{R\{a^2+(l-a)^2\}}{l^2J_x}} \quad \cdots\cdots(16)'$$

$$f_{XX}=\frac{1}{EJl^2}\left[\left(\frac{\alpha^2a^3}{3}\right)+2b\left\{(lR)^2-l^2R\alpha+\frac{1}{3}\alpha^2(3a^2+6ab+4b^2)\right\}+\frac{\alpha^2a}{3}\left\{l^2+l(a+2b)+(a+2b)^2\right\}\right]+\frac{R}{EJ_zl^2}\left[\frac{2}{3}l^2R^2-l^2R\alpha+\alpha^2\left\{a^2+(l-a)^2\right\}\right] \quad \cdots\cdots(17)'$$

If more accuracy is desired, shearing deformation of arms may be added, resulting in

$$f_{XX'}=\frac{12(R-d)}{5Gwh}+f_{XX} \quad \cdots\cdots(20)$$

where d is the outside diameter of pin and journal, while w and h are side lengthes of the rectangular arm section parallel to Z- and X-axis respectively.

3. 2. 2 Influence numbers under loading around X-axis.

Similarly the indeterminate moment around Y-axis at B-end, β, is derived and then the influence number $f_{\Theta\Theta}$ is calculated. Especially for the case $J_1=J_2=J$, $J_j=J_p$ and $a_1=a_2=a$,

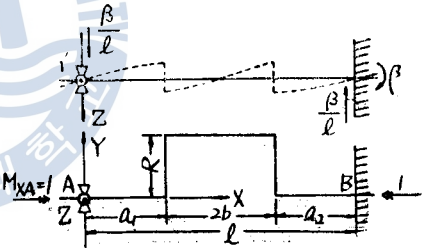

Fig. 4 Force and moment induced by the loading around X-axis

$$\beta=\frac{\frac{2Rb}{lGJ_p}+\frac{R^2}{lEJ_x}}{\frac{l}{3EJ}+\frac{2bR^2}{l^2GJ_p}+\frac{R\{a^2+(l-a)^2\}}{l^2GJ_p}+\frac{2R^3}{3l^2EJ_x}} \quad \cdots\cdots(21)$$

$$f_{\Theta\Theta}=\frac{2}{GJ_p}\left\{a+\frac{b}{l^2}(l-\beta R)^2\right\}+\frac{\beta^2l}{3EJ}+\frac{2R}{EJ_xl^2}(l^2-l\beta R+\frac{1}{3}\beta^2R^2)+\frac{\beta^2R}{GJ_pl^2}\{a^2+(a-l)^2\} \quad \cdots\cdots(22)$$

$$f_{\Psi\Theta}=0 \quad \cdots\cdots(23)$$

Where G is the modulus of rigidity, J_i and J_p are polar moments of inertia of journal

and pin section respectively, J_x, J_y are moments of inetia of arm section about X-, Y-axis respectively and $J_y = cwh$, c being a constant depending on the ratio w/h.

3. 2. 3 Influence numbers under loading around Y-axis.

In this case also, the indeterminate moment around Y-axis at B-end, γ, is derived and influence numbers, $f_{\Phi\Phi}$, $f_{\Theta\Phi}$ are calculated. For the case, $J_1 = J_2 = J$ and $a_1 = a_1 = a$,

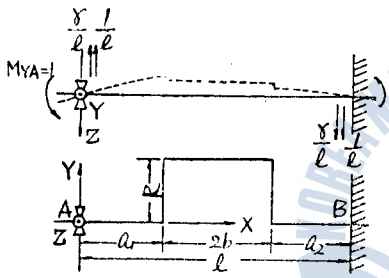

Fig. 5 Force and moment induced by the loading around Y-axis

$$\gamma = \frac{-\left[-\frac{l}{6EJ} + \frac{2Ra(a-l)}{GJ_y l^2} + \frac{2R^3}{3EJ_x l^2}\right]}{\frac{l}{3EJ} + \frac{2bR^2}{GJ_p l^2} + \frac{R\{a^2+(l-a)^2\}}{l^2 GJ_y} + \frac{2bR^2}{GJ_p l^2} + \frac{2R^3}{3EJ_x l^2}} \quad \cdots\cdots(24)$$

$$f_{\Phi\Phi} = \frac{l}{3EJ}\left\{1+\gamma(\gamma-1)\right\} + \frac{2bR^2(1+\gamma)^2}{GJ_p l^2} + \frac{R}{GJ_y l^2}[\{l-(1+\gamma)a\}^2 + \{l\gamma-(1+\gamma)a\}^2] + \frac{2R^3(1+\gamma)^2}{3EJ_x l^2} \quad \cdots\cdots(25)$$

$$f_{\Theta\Phi} = \frac{\beta l(1-2\gamma)}{6EJ} + \frac{2bR(1+\gamma)(l-\beta R)}{GJ_p l^2} + \frac{R\beta}{GJ_y l^2}[a\{l-(1+\gamma)a\} + (a-l)\{l\gamma - (1+\gamma)a\}] + \frac{R^2(\gamma+1)(3l-2\beta R)}{3EJ_x l^2} \quad (26)$$

$$f_{\Psi\Phi} = 0 \quad \cdots\cdots(27)$$

3. 2. 4 Influence numbers under loading around Z-axis.

After deriving the indeterminate moment around Z-axis, ρ, influence numbers, $f_{\Psi\Psi}$ and $f_{X\Psi}$ are calculated. For the case $J_1 = J_2 = J$ and $a_1 = a_1 = a$,

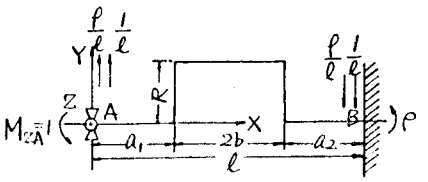

Fig. 6 Force and moment induced by the loading around Z-axis

$$\rho = \frac{-\left\{-\frac{l}{6J} + \frac{2Ra(a-l)}{J_x l^2}\right\}}{\frac{l}{3J} + \frac{R\{a^2+(l-a)^2\}}{J_x l^2}} \quad \cdots\cdots(28)$$

$$f_{\Psi\Psi} = \frac{l}{EJ}\left\{\frac{1}{3}(\rho+1)^2 - \rho\right\} + \frac{R}{EJ_x l^2}[\{l-(\rho+1)a\}^2 + \{l\rho-(\rho+1)a\}^2] \quad \cdots(29)$$

$$f_{X\Psi} = \frac{\alpha a}{EJl^2}\left[\frac{1+\rho}{3}\left\{a^2+l^2+l(a+2b) + (a+2b)^2\right\} - l^2\right] + \frac{2b}{EJl^2}[l^2R - (a+b)l\{(1+\rho)R+\alpha\} + \frac{\alpha(1+\rho)}{3}\left\{\{(a+2b)^2 + a(a+2b) + a^2\}\right] + \frac{R}{EJ_x l^2}\left[\left\{l - (1+\rho)a\right\}\left(\frac{lR}{2} - \alpha a\right) + \left\{l\rho - (\rho+1)a\right\}\left\{\alpha(l-a) - \frac{lR}{2}\right\}\right] \quad \cdots\cdots(30)$$

3. 3 Stiffness matrix of a single throw which is in plane xy.

If X-, Y-, Z-axis of the unit throw coincide with x-, y-, z-axis respectively, the influence numbers derived as above lead to a relation of forces and displacements as

$$\begin{pmatrix} x_A \\ \theta_A \\ \varphi_A \\ \psi_A \end{pmatrix} = \begin{pmatrix} f_{XX} & 0 & 0 & f_{X\Psi} \\ 0 & f_{\Theta\Theta} & f_{\Theta\Phi} & 0 \\ 0 & f_{\Phi\Theta} & f_{\Phi\Phi} & 0 \\ f_{\Psi X} & 0 & 0 & f_{\Phi\Psi} \end{pmatrix} \begin{pmatrix} F_A \\ M_{XA} \\ M_{YA} \\ M_{ZA} \end{pmatrix} \quad \cdots\cdots(31)$$

or $\{X_A\} = [F_{AA}]\{F_A\}$ $\cdots\cdots(31)$

where $[F_{AA}]$ is a symmetric matrix, and may be inverted into $[K_{AA}]$ which is a stiffness matrix in case of B-end fixed and A-end loaded:

$$[K_{AA}] = \begin{pmatrix} k_{XX} & 0 & 0 & k_{X\Psi} \\ 0 & k_{\Theta\Theta} & k_{\Theta\Phi} & 0 \\ 0 & k_{\Phi\Theta} & k_{\Phi\Phi} & 0 \\ k_{\Psi X} & 0 & 0 & k_{\Psi\Psi} \end{pmatrix} \quad \cdots\cdots(32)$$

where

$$k_{XX} = \frac{f_{\Psi\Psi}}{f_{XX}f_{\Psi\Psi} - (f_{X\Psi})^2}, \quad k_{X\Psi} = k_{\Psi X} = \frac{-f_{\Psi X}}{f_{XX}f_{\Psi\Psi} - (f_{X\Psi})^2}, \quad k_{\Theta\Theta} = \frac{f_{\Phi\Phi}}{f_{\Theta\Theta}f_{\Phi\Phi} - (f_{\Theta\Phi})^2}$$

$$k_{\Theta\Phi} = k_{\Phi\Theta} = \frac{-f_{\Theta\Phi}}{f_{\Theta\Theta}f_{\Phi\Phi} - (f_{\Theta\Phi})^2},$$

$$k_{\Phi\Phi} = \frac{f_{\Theta\Theta}}{f_{\Theta\Theta}f_{\Phi\Phi} - (f_{\Theta\Phi})^2},$$

$$k_{\Psi\Psi} = \frac{f_{XX}}{f_{XX}f_{\Psi\Psi} - (f_{X\Psi})^2} \quad \cdots\cdots(33)$$

or $\{F_A\} = [K_{AA}]\{X_A\}$ $\cdots\cdots(32)$

The reaction matrix at B-end, $[K_{BA}]$, is derived from the relations equating external forces;

$$\sum F = F_A + F_B = 0$$

$$\sum M_X = M_{XA} + M_{XB} = 0$$

$$\sum M_y = \frac{\beta}{l} \cdot M_{XA} \cdot l + M_{YA} - \frac{(1+\gamma)}{l} \cdot M_{YA} l + M_{YB} = 0$$

$$\sum M_z = -\alpha/l \cdot F_A \cdot l + M_{ZA} - \frac{(1+\rho)}{l} \cdot M_{ZA} \cdot l + M_{ZA} = 0$$

or

$$\begin{pmatrix} F_B \\ M_{XB} \\ M_{YB} \\ M_{ZB} \end{pmatrix} = \begin{pmatrix} -1 & 0 & 0 & 0 \\ 0 & -1 & 0 & 0 \\ 0 & -\beta & \gamma & 0 \\ \alpha & 0 & 0 & \rho \end{pmatrix} \begin{pmatrix} F_A \\ M_{XA} \\ M_{YA} \\ M_{ZA} \end{pmatrix} \quad \cdots\cdots(34)$$

From (33)′ and (34)

$$[K_{BA}] = \begin{pmatrix} -k_{XX} & 0 & 0 & -k_{X\Psi} \\ 0 & -k_{\Theta\Theta} & -k_{\Theta\Phi} & 0 \\ 0 & (-\beta k_{\Theta\Theta} + \gamma k_{\Phi\Theta}) & (-\beta k_{\Theta\Phi} + \gamma k_{\Phi\Phi}) & 0 \\ (\alpha k_{XX} + \rho k_{\Psi X}) & 0 & 0 & (\alpha k_{X\Psi} + \rho k_{\Psi\Psi}) \end{pmatrix} \quad \cdots\cdots(35)$$

As for stiffness matrices in the case of reversed boundary conditions: A-end fixed and B-end loaded, every element has definitely the same absolute size as the corresponding one of $[K_{AA}]$ and $[K_{BA}]$, but not always the same sign. They are

$$[K_{BB}] = \begin{pmatrix} k_{XX} & 0 & 0 & k_{X\Psi} \\ 0 & k_{\Theta\Theta} & -k_{\Theta\Phi} & 0 \\ 0 & -k_{\Phi\Theta} & k_{\Phi\Phi} & 0 \\ k_{\Psi X} & 0 & 0 & k_{\Psi\Psi} \end{pmatrix} \quad (36)$$

and

$$[K_{AB}] = \begin{pmatrix} -k_{XX} & 0 & 0 & -k_{X\Psi} \\ 0 & -k_{\Theta\Theta} & k_{\Theta\Phi} & 0 \\ 0 & (\beta k_{\Theta\Theta} - \gamma k_{\Theta\Phi}) & (-\beta k_{\Theta\Phi} + \gamma k_{\Phi\Phi}) & 0 \\ (\alpha k_{XX} + \rho k_{\Psi X}) & 0 & 0 & (\alpha k_{X\Psi} + \rho k_{\Psi\Psi}) \end{pmatrix} \quad \cdots\cdots(37)$$

Combination of these matrices gives an overall stiffness matrix as

$$[K^{AB}] = \begin{pmatrix} K_{AA} & \vdots & K_{AB} \\ \cdots\cdots & \cdot & \cdots\cdots \\ K_{BA} & \vdots & K_{BB} \end{pmatrix} \quad \cdots\cdots(38)$$

where $[K^{AB}]$ is a symmetric matrix, although its diagonal elements from upper right to lower left appear unsymmetric. Actually numerical calculation proves the symmetry, giving $-k_{X\Psi} = \alpha\, k_{XX} + \rho k_{\Psi X}$, and

$k_{\Theta\Phi} = -\beta k_{\Theta\Theta} + \gamma k_{\Theta\Phi}$.

This symmetry-characteristic of $[K^{AB}]$ serves to check derivation error of the matrix elements.

3.4 Stiffness matrix of a single throw which is not in plane xy.

As shown in Fig. 7, give plane XY a negative rotation around the common axis X or x by ε from plane xy. In this case, stiffness matrix based on y-and z-axis is not equal to $[K_{AA}]$ in Section 3.3, but may be derived considering the effect of rotation on the element of $[K_{AA}]$.

Among the six elements, k_{XX} and $k_{\Theta\Theta}$ are unchanged, as x and X are coincident. Projection onto y-and z-axis of a moment around z-axis amounting to $k_{\Psi X}$ multiplied by a unit X- or x-displacement gives

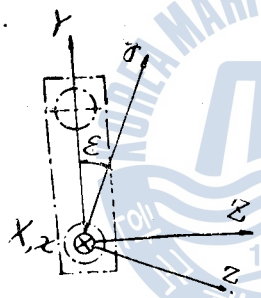

Fig. 7 The throw deviates from plane xy

$$k_{\varphi x} = k_{\Psi X} \sin\varepsilon \quad \cdots\cdots(39)$$

$$k_{\phi x} = k_{\Psi X} \cos\varepsilon \quad \cdots\cdots(40)$$

Similary, projection of $k_{\Phi\Theta}$ multiplied by a unit displacement around X or x on to y- and z-axis gives

$$k_{\varphi\theta} = k_{\Phi\Theta} \cos\varepsilon \quad \cdots\cdots(41)$$

$$k_{\phi\theta} = k_{\Phi\Theta} (-\sin\varepsilon) \quad \cdots\cdots(42)$$

A unit angular displacement around y-axis may be composed of Φ-component, $\cos\varepsilon$, and Ψ-component, $\sin\varepsilon$. These components may be derived from moment $k_{\Phi\Phi}\cos\varepsilon$ around Y and moment $k_{\Psi\Psi}\sin\varepsilon$ around Z respectively. Finally, projection of the moments on to y- and z-axis gives

$$k_{\varphi\varphi} = k_{\Phi\Phi}\cos^2\varepsilon + k_{\Psi\Psi}\sin^2\varepsilon \quad \cdots\cdots(43)$$

$$k_{\phi\varphi} = \sin\varepsilon\cos\varepsilon(-k_{\Phi\Phi} + k_{\Psi\Psi}) \quad \cdots\cdots(44)$$

Similarly a unit displacement around Z-axis leads to $k_{\varphi\phi} = k_{\phi\varphi}$ and

$$k_{\phi\phi} = k_{\Phi\Phi}\sin^2\varepsilon + k_{\Psi\Psi}\cos^2\varepsilon \quad \cdots\cdots(45)$$

Let $\cos\varepsilon = \lambda$ and $\sin\varepsilon = \mu$

Then, the stiffness matrices based on y-and z-axis are as follows:

$$[\bar{K}_{AA}] = \begin{pmatrix} k_{XX} & 0 & \mu k_{X\Psi} & \lambda k_{X\Psi} \\ 0 & k_{\Theta\Theta} & \lambda k_{\Theta\Phi} & -\mu k_{\Theta\Phi} \\ \mu k_{\Psi X} & \lambda k_{\Phi\Theta} & (\lambda^2 k_{\Phi\Phi} + \mu^2 k_{\Psi\Psi}) & (-\lambda\mu k_{\Phi\Phi} + \mu\lambda k_{\Psi\Psi}) \\ \lambda k_{\Psi X} & -\mu k_{\Phi\Theta} & (-\mu\lambda k_{\Phi\Phi} + \lambda\mu k_{\Psi\Psi}) & (\mu^2 k_{\Phi\Phi} + \lambda^2 k_{\Psi\Psi}) \end{pmatrix} \quad \cdots\cdots(46)$$

and

$$[\bar{K}_{BA}] = \begin{pmatrix} -k_{XX} & 0 & -\mu k_{X\Psi} & -\lambda k_{X\Psi} \\ 0 & -k_{\Theta\Theta} & -\lambda k_{\Theta\Phi} & \mu k_{\Theta\Phi} \\ \mu(\alpha k_{XX} + \rho k_{\Psi X}) & \lambda(-\beta k_{\Theta\Theta} + \gamma k_{\Theta\Phi}) & \lambda^2(-\beta k_{\Theta\Phi} + \gamma k_{\Phi\Phi}) + \mu^2(\alpha k_{X\Psi} + \rho k_{\Psi\Psi}) & -\mu\lambda(-\beta k_{\Theta\Phi} + \gamma k_{\Phi\Phi}) + \lambda\mu(\alpha k_{X\Psi} + \rho k_{\Psi\Psi}) \\ \lambda(\alpha k_{XX} + \rho k_{\Psi X}) & -\mu(-\beta k_{\Theta\Theta} + \gamma k_{\Theta\Phi}) & \lambda\mu(\beta k_{\Theta\Phi} + \gamma k_{\Phi\Phi}) + (\mu\lambda\alpha k_{X\Psi} + \rho k_{\Phi\Phi}) & \mu^2(-\beta k_{\Theta\Phi} + \gamma k_{\Phi\Phi}) + \lambda^2(\alpha k_{X\Psi} + \rho k_{\Psi\Psi}) \end{pmatrix} \quad \cdots\cdots(47)$$

$$[\bar{K}_{BB}] = \begin{pmatrix} k_{XX} & 0 & \mu k_{X\Psi} & \lambda k_{X\Psi} \\ 0 & k_{\Theta\Theta} & -\lambda k_{\Theta\Phi} & \mu k_{\Theta\Phi} \\ \mu k_{\Psi X} & -\lambda k_{\Phi\Theta} & (\lambda^2 k_{\Phi\Phi} + \mu^2 k_{\Psi\Psi}) & (-\lambda\mu k_{\Phi\Phi} + \mu\lambda k_{\Psi\Psi}) \\ \lambda k_{\Psi X} & \mu k_{\Phi\Theta} & (-\mu\lambda k_{\Phi\Phi} + \mu\lambda k_{\Psi\Psi}) & (\mu^2 k_{\Phi\Phi} + \lambda^2 k_{\Psi\Psi}) \end{pmatrix} \quad \cdots\cdots(48)$$

$$[\bar{K}_{AB}]=\begin{pmatrix} -k_{XX} & 0 \\ 0 & -k_{\Theta\Theta} \\ \mu(\alpha k_{XX}+\rho k_{\Psi X}) & \lambda(\beta k_{\Theta\Theta}-\gamma k_{\Theta\Phi}) \\ \lambda(\alpha k_{XX}+\rho k_{\Psi X}) & -\mu(\beta k_{\Theta\Theta}-\gamma k_{\Theta\Phi}) \end{pmatrix}$$

$$\begin{pmatrix} -\mu k_{X\Psi} \\ \lambda k_{\Theta\Phi} \\ \lambda^2(-\beta k_{\Theta\Phi}+\gamma k_{\Phi\Phi})+\mu^2(\alpha k_{X\Psi}+\rho k_{\Psi\Psi}) \\ \mu\lambda(-\beta k_{\Theta\Phi}+\gamma k_{\Phi\Phi})+\lambda\mu(\alpha k_{X\Psi}+\rho k_{\Psi\Psi}) \\ -\lambda k_{X\Psi} \\ -\mu k_{\Theta\Phi} \\ \lambda\mu(-\beta k_{\Theta\Phi}+\gamma k_{\Phi\Phi})+\mu\lambda(\alpha k_{X\Psi}+\rho k_{\Psi\Psi}) \\ \mu^2(-\beta k_{\Theta\Phi}+\gamma k_{\Phi\Phi})+\lambda^2(\alpha k_{X\Psi}+\rho k_{\Psi\Psi}) \end{pmatrix} \quad \cdots\cdots(49)$$

Combination of the above matrices gives

$$[\bar{K}^{AB}]=\begin{pmatrix} \bar{K}_{AA} & \vdots & \bar{K}_{AB} \\ \cdots & \cdot & \cdots \\ \bar{K}_{BA} & \vdots & \bar{K}_{BB} \end{pmatrix} \quad \cdots\cdots(50)$$

Matrix (50) is also symmetric as (38).

3.5 Stiffiness matrix of a round bar.

Intermediate shaft, thrust shaft, propeller shaft and coupling parts of the crankshaft may be represented by simple round bars.

The stiffness matrix for each of them has the expression as

$$[K_{AA}]=\begin{pmatrix} EA/l & 0 & 0 & 0 \\ 0 & GJ_p/l & 0 & 0 \\ 0 & 0 & 4EJ/l & 0 \\ 0 & 0 & 0 & 4EJ/l \end{pmatrix}=[K_{BB}] \quad \cdots\cdots(51)$$

$$[K_{BA}]=\begin{pmatrix} -EA/l & 0 & 0 & 0 \\ 0 & -GJ_p/l & 0 & 0 \\ 0 & 0 & 2EJ/l & 0 \\ 0 & 0 & 0 & 2EJ/l \end{pmatrix}[K_{AB}] \quad \cdots\cdots(52)$$

$$[K^{AB}]=\begin{pmatrix} K_{AA} & \vdots & K_{AB} \\ \cdots & \cdot & \cdots \\ K_{BA} & \vdots & K_{BB} \end{pmatrix} \quad \cdots\cdots(53)$$

Where l and A are the length and sectional area of the bar and other symbols are the same as above.

Except coupling parts they may be supposed to have only two degrees of freedom; x-and θ-displacement, then Eqs. (51), (52) and (53) may be reduced to matrices with two columns and two rows.

4. Numerical analysis and comparison of calculated to measured values.

4.1 Specifications of analyzed engines.

Assumed name of ship	S	B	M
Kind of ship	Cargo ship	Cargo ship	Oil tanker
Gross tonnage (₸)	8,515	6,700	72,000
Type of main engine	2-cycle single-acting cross-head type.		
No. of cylinders-bore × stroke(mm)	8−720×1,250	9×749−1,600	10−860×1,600
Out-put (P.S.)× speed(R.P.M.)	6,100×137	8,000×110.5	23,000×115
Brake mean effective pressure(kg/cm²)	5.98	6.50	10.91
Firing order	1-8-3-4-7-2-5-6	1-8-3-6-5-4-7-2-9	1-8-6-5-3-10-4-2-9-7

Type of crankshaft	Forged steel semi-built×2pcs.	Cast steel full-built×2pcs.	Forged steel semi-built×2pcs.
Propeller	ϕ 5,100×4 blades	ϕ 5,800×4 blades	ϕ 6,650×6 blades
Thrust block	Bolted to engine block	Bolted to engine block	Founded on engine room floor
Balancing weight	None	Attached to No. 1, 4, 5, 8 throw	None
Engine position	Midship	Midship	Aftship
Skelton diagram of crankshaft	Fig. 8	Fig. 9	Fig. 10

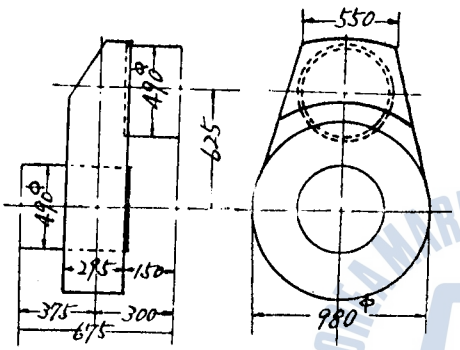

Fig. 8 Crankshaft skelton diagram of Ship S

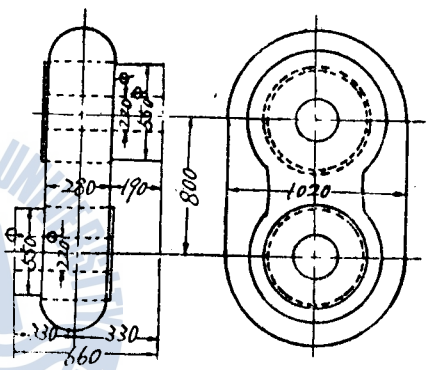

Fig. 9 Crankshaft skelton diagram of Ship B

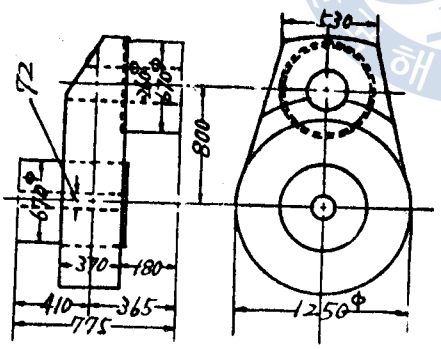

Fig. 10 Crankskaft skelton diagram of Ship M

4. 2 Numerical Calculation.

Every of the three shaftings, S, B and M was divided into 15 equivalent inertia bodies and all matrix elements were calculated with a digital computer HITAC 5020E in order to built up square matrices of order 50, 52 and 54 for S, B and M respectively. They were solved on the same computer in 58, 67 and 73 seconds respectively, giving 50, 52 and 54 eigenvalues (natural frequencies) and corresponding normalized eigenvectors (modes) successively printed. The calculated data are shown in Table 1, 2 and 3. Table 1 shows calculated indeterminate fixing moments defined in Fig, 3, 4, 5 and 6. Table 2 shows calculated influence numbers. Table 3 shows calculated stiffnesses.

Every mass moment of inertia amounts to the same as that derived at conventional torsional vibration analysis, while the entrained water mass is supposed to be 60% of

Table 1. Calculated indeterminate fixing moments defined in Fig. 3, 4, 5, 6

cm-kg

Ship	α $\times 10^2$	β	γ	ρ
S	0.4766484	0.3622307	0.3358176	0.5969501
B	0.6300806	0.3336151	0.2690116	0.5762000
M	0.6292483	0.3524626	0.1391534	0.5050736

Table 2. Calculated influence numbers cm/kg, rad/cm-kg

Ship	$f_{XX} \times 10^{-6}$	$f_{X\Psi}=f_{\Psi X} \times 10^{-8}$	$f_{\Theta\Theta} \times 10^{-9}$	$f_{\Theta\Phi}=f_{\Phi\Theta} \times 10^{-10}$	$f_{\Phi\Phi} \times 10^{-9}$	$f_{\Psi\Psi} \times 10^{-9}$
S	0.4496945	0.3368360	0.3045998	0.9203019	0.1687456	0.1128526
B	0.7174846	0.5144534	0.1936225	0.8283117	0.1814925	0.1286133
M	0.3064232	0.2035474	0.1095262	0.3939575	0.083882	0.0515970

Table 3. Calculated stiffnesses kg/cm, cm-kg/rad

Ship	$k_{XX} \times 17^7$	$k_{X\Psi}=k_{\Psi X} \times 10^8$	$k_{\Theta\Theta} \times 10^{10}$	$k_{\Theta\Phi}=k_{\Phi\Theta} \times 10^{10}$	$k_{\Phi\Phi} \times 10^{10}$	$k_{\Psi\Psi} \times 10^{11}$
S	0.2864036	-0.8548406	0.3930685	-0.2143710	0.7095218	0.1141259
B	0.1954258	-0.7817030	0.6417693	-0.2928964	0.6846616	0.1090205
M	0.4422336	-1.7445880	1.0985990	-0.5169265	1.4343540	0.2626329

the propeller.

4.3 Natural frequencies and vibration modes.

4.3.1 Natural frequencies

The calculated and measured natural frequencies of Ship S, B and M are shown in Table 4, 5 and 6 respectively, where the stars indicate indistinct measurements.

In author's calculation the stiffness of thrust block was iteratively adjusted so as to lessen the differences between calculated and

Table 4. Comparison of calculated to measured frequencies of Ship S

Mode	Measured values	Conventional Holzer method $k_o=0.60\times10^7 kg/cm$ according to Anderson's			Author's method. Author iteratively derive $k_o=0.90\times10^7$ kg/cm	
		Torsional	Axial	Cal./Meas.	Calculated	Cal./Meas.
1-node Tor.	V.P.M.☆	191.68			189.28	
0-node Axi.	985		969.41	98%	963.79	98%
1-node Axi.	1064		1103.54	104	1034.46	97
2-node Tor.	1101	1093.68		99	1057.19	96

Table 5. Comparison of calculated to measured frequencies of Ship B.

Mode	Measured values	Conventional Holzer method $k_o=0.20\times10^7 kg/cm$ according to Anderson's			Author's method. Author iteratively derive $k_o=0.20\times10^7$ kg/cm	
		Torsional	Axial	Cal./Meas.	Calculated	Cal./Meas.
1-node Tor.	V.P.M☆	149.60			144.78	
0-node Axi.	513		549.48	107%	495.57	97%
1-node Axi.	765		769.94	101	753.65	98
2-node Tor.	844	827.03		98	814.44	97

Table 6. Comparison of calculated to measured frequencies of Ship M

Mode	Measured values	Conventional Holzer method $k_o=0.221\times10^7 kg/cm$ according to Anderson's			Author's method. Author iteratively derive $k_o=0.250\times10^7$ km/cm	
		Torsional	Axial	Cal./Meas.	Calculated	Cal./Meas.
	V.P.M					
1-node Tor.	376	388.30		103%	375.03	100%
0-node Axi.	628		660.00	105	623.98	99
2-node Tor.	1017	1053.40		104	1015.18	100
1-node Axi.	☆		1376.40		1364.02	

measured frequencies and modes. For the calculation of the axial vibration by Holzer method, Anderson's formula was used, which gave the best result among various empirical formulae. [1][2][3][8][9][10] Provided the thrust block stiffness is 0.60×10^7kg/cm, the nodeless axial natural frequency of Ship S(1st mode) is about 2% smaller than the measured one and that of one-node (2nd mode) is about 4% larger than the measured one. Supposing a stiffer thrust block in order to correct the calculated nodeless frequency, the difference between the calculated one-node frequency and measured one becomes still bigger.

Table 7 Estimation of thrust block stiffness. kg/cm

Ship	Formula (12)	Formula (13)	The iteratively derived values.
S	0.905×10^7	0.912×10^7	0.900×10^7
B	0.183×10^7	0.215×10^7	0.200×10^7
M	0.240×10^7	0.279×10^7	0.250×10^7

Table 7 shows stiffness estimations derived from formula (12), (13) and the above mentioned iteration.

Fig. 11 shows the so-called frequency spectrum, the relation between frequency and thrust block stiffness. Seven natural frequencies of Ship S and six of B, which come into question in view of the crankshaft vibration, are plotted. The interesting feature of Ship S is the adjacent location of the one-node axial frequency to the two-node torsional one, what suggests a strong coupled axial-torsional vibration at this engine speed. Actually the measured result on board backs up this assumption. These frequencies scarcely depend on the thrust block stiffness as it is shown in Fig. 11, because the node of one-node axial vibration is located close to the thrust block. In such a case, nobody can shift the one-node frequency, i.e. the strong,

coupled axial-torsional frequency by changing the thrust block stiffness.

As for Ship B, the one-node axial frequency approaches the two-node torsional with increasing block stiffness up to about 0.50×10^{7} kg/cm, where the two intersect. This suggests a strong, coupled vibration and a possible shaft danger nearby. In this case also, seperation of the two from each other is difficult, so that a remarkable coupled vibration appears, even when the thrust block stiffness is fairy below the dangerous measure.

By making and discussing such a spectrum in the design stage of a ship, it would be possible in advance to find remedy for coupled vibration troubles or to select the most suitable thrust block stiffness. On the other hand, the effect of the thrust block stiffness on uncoupled torsional vibration is little. In addition, Ship M did not show a coupled vibration as S or M.

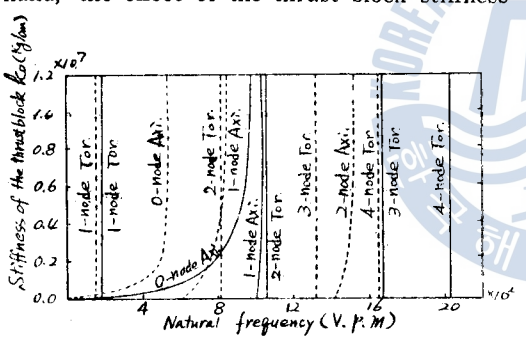

Fig. 11 Frequency spectrum

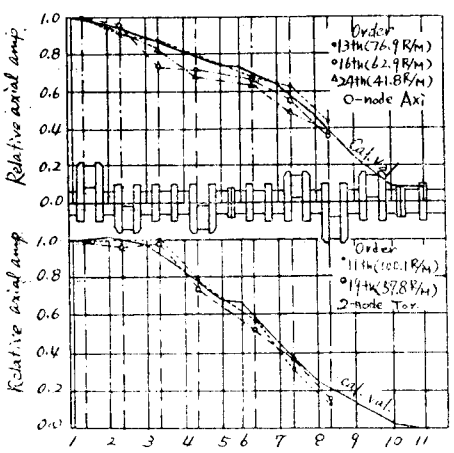

Fig. 12 Relative axial amp. of Ship S at crankshaft

4. 3. 2 Vibration modes.

The upper part of Fig. 12 shows nodeless axial vibration modes of Ship S. The 13th order, measured mode agrees best with the author's calculation but the others deviate a little at No. 3 and No. 4 measuring point. The figure below shows modes of axial vibration accompanied with the two node torsional vibration, which has never been analyzed so far. The calculated mode excellently agrees with measured ones, which appear to be nearly constant between Pt. 1 and Pt. 3, thence to descend.

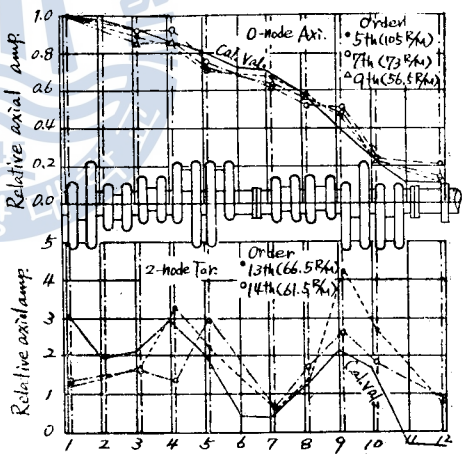

Fig. 13 Relative axial amp. of Ship B at crankshaft

The upper part of Fig. 13 shows nodeless axial vibration modes of Ship B, where the calculated mode agrees on the whole with measured ones.

The axial vibration modes of the figure below accompanied with two-node torsional vibration, are rather singular, compared with those shown above. The ordinate represents the measured axial amplitude in mm and also

the reduced calculation based on the relation, equating the torsional calculated stress at Pt. 8 with the corresponding measurement. Although the comparison is not proper due to lack of data at the second throw, the calculated mode on the whole resembles the measured one except the fore-end. This deviation may be attributed to incomplete description of experimental system, which had a plunger type bilge pump at the fore-end, while the calculation has assumed a pumpless system.

Table. 8, 9 and 10 show relative amplitudes

Table 8 Comparison of crankshaft fore-end amplitudes of Ship S.

Mode	x	$d\theta/2$	$d\varphi/2$	$d\psi/2$
1-node Tor.	0.540×10^{-2}	1.000	0.565×10^{-3}	0.342×10^{-3}
0-node Axi.	1.000	0.235×10^{-1}	0.237×10^{-2}	0.101×10^{-1}
1-node Axi.	1.000	0.109	0.127×10^{-2}	0.125×10^{-1}
2-node Tor.	0 421	1.000	0.191×10^{-1}	0.537×10^{-2}
3-node Tor.	0.201	1.000	0.436×10^{-2}	0.313×10^{-1}
4-node Tor.	0.439	1.000	0.676×10^{-1}	0.602×10^{-1}
2-node Axi.	1.000	0.781×10^{-1}	0.119×10^{-1}	0.899×10^{-1}

Table 9 Comparison of crankshaft fore-end amplitudes of Ship B.

Mode	x	$d\theta/2$	$d\varphi/2$	$d\psi/2$
1-node Tor.	0.512×10^{-2}	1.000	0.657×10^{-3}	0.719×10^{-3}
0-node Axi.	1.000	0.483×10^{-2}	0.199×10^{-2}	0.250×10^{-2}
1-node Axi.	1.000	0.597×10^{-1}	0.621×10^{-2}	0.547×10^{-2}
2-node Tor.	0.187	1.000	0.203×10^{-1}	0.242×10^{-1}
3-node Tor.	0.407	1.000	0.515×10^{-1}	0.669×10^{-1}
2-node Axi.	1.000	0.157×10^{-1}	0.222×10^{-1}	0.263×10^{-1}
4-node Tor.	0.486	1.000	0.872×10^{-1}	0.112

Table 10 Comparison of crankshaft fore-end amplitudes of Ship M

Mode	x	$d\theta/2$	$d\varphi/2$	$d\psi/2$
1-node Tor.	0.142	1.000	0.259×10^{-2}	0.255×10^{-2}
0-node Axi.	1.000	0.161×10^{-2}	0.191×10^{-3}	0.437×10^{-2}
2-node Tor.	0.481×10^{-1}	1.000	0.191×10^{-1}	0.174×10^{-1}
1-node Axi	1.000	0.904×10^{-2}	0.553×10^{-3}	$0.209\times10_{-1}$
3-node Tor.	0.931	1.000	0.689×10^{-1}	0.925×10^{-1}
2-node Axi.	1.000	0.774×10^{-1}	0.469×10^{-2}	0.466×10^{-1}
4-node Tor.	1.244	1.000	0.145	0.204

of x, θ, φ and ψ of the crankshaft fore-end, where θ, φ and ψ were multiplied by the radius of journal, for the sake of vivid comparison of torsional, lateral and another lateral mode with the axial one on the same scale. It is clearly seen, that φ- and ψ-amplitude become relatively larger as the natural frequency increases.

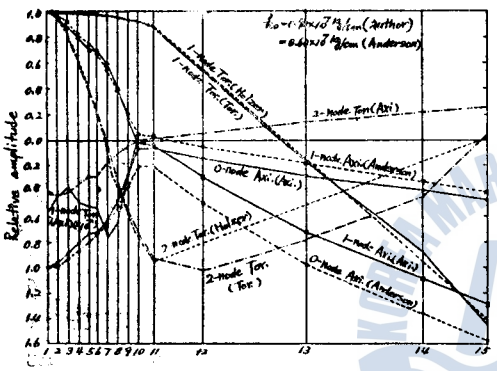

Fig. 14 Relative amplitudes Ship S (calculated)

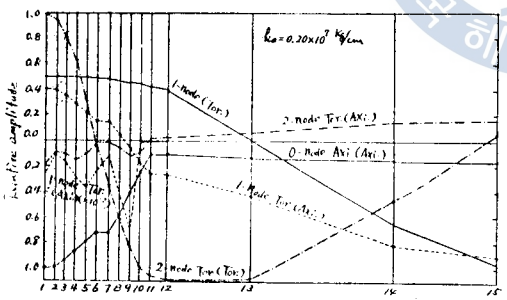

Fig. 15 Relative amplitudes Ship B (calculated)

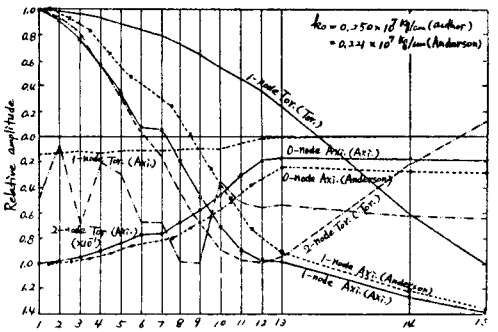

Fig. 16 Relative amplitudes Ship M (calculated)

ordinate represents the ratio of x or $d\theta/2$ to the fore-end torsional amplitude in case of torsional and axial-torsional vibration and also the ratio of x to the fore-end axial amplitude in case of axial vibration. In Fig. 14 and 16 are shown also curves derived from the conventional Holzer method, using Anderson's formula for axial stiffness and engine-maker-'s own empirical formulae for torsional stiffness.

4. 3. 3 The influence of crank throw arrangement on crankshaft vibration.

It is expected that the arrangement of crank throw affects the vibration of crankshaft. Here will be investigated the crankshaft without any balance weight for Ship S.

Three kinds of firing order shown in Table 11 are adopted in practice for 2 cycle single acting marine diesel engine in Japan.

Table 11 Firing order of 2-cycle single acting 8-cylinder engine

Kinds of firing	Firing order	No. of examples	Remarks
A	1-8-3-4-7-2-5-6	6	Firing order ship S
B	1-8-3-5-2-7-4-6	2	
C	1-7-3-5-4-6-2-8	1	

Fig. 14, 15 and 16 show relative amplitude curves of Ship S, B and M respectively. The

Table 12 shows smallest natural frequencies

Table 12 Natural frequencies for various firing orders for Ship S.

$k_o = 0.90 \times 10^7\ kg/cm$

Kinds of firing	1-node torsional	0-node axial	1-node axial	2-node torsional	3-node torsional	4-node torsiona	2-node axial
	V.P.M.						
A	189.28	963.79	1034.46	1057.19	1683.47	2129.65	2792.04
B	189.31	932.75	1024.72	1088.99	1683.05	2143.50	2708.57
C	189.28	943.73	1027.29	1080.77	1683.67	2139.68	2759.38

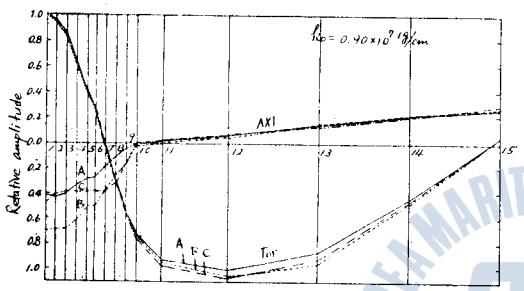

Fig. 17 2-node torsional amplitudes and the coupled axial ones for various firing orders of Ship S

corresponding to the three firing orders. Among them, two-node torsional vibration, which often couples large axial vibration on midship engines, is shown in Fig. 17.

From Table 12 and Fig. 17 it can be deduced that the effect of firing order (arrangement of crank throws) is generally stronger on axial vibrations than on torsional vibration, except those which accompany strong axial vibrations. Hence it is possible to reduce additional stressing due to axial vibration, choosing an appropriate firing order. Anyhow such a means arises, provided the coupled torsional-axial vibration has been solved.

5. Application to the uncoupled vibration analysis.

The stiffness matrix of uncoupled vibrating system is derived with the same method for a coupled vibrating system as follows

$$[K^{1,p}] = \begin{pmatrix} k_1 & -k_1 & & & \\ -k_1 & (k_1+k_2) & -k_2 & & 0 \\ & \ddots & \ddots & \ddots & \\ & -k_i & (k_i+k_{i+1}) & -k_{i+1} & \\ & & \ddots & \ddots & \ddots \\ 0 & & -k_{p-1} & (k_{p-1}+k_p) & -k_p \\ & & & \ddots & \ddots \\ & & & -k_p & k_p \end{pmatrix} \quad \cdots\cdots(54)$$

k_i are uncoupled axial or torsional stiffnesses which are derived from formulae 55, 56 or other empirical formulae and k_o represents the thrust blcok stiffness.

Axial influence number:

$$f_X = \frac{2Rb}{EJ}\left(R - \frac{2\xi_X}{3}\right) + \frac{2R^2}{3EJ_z}(R - \xi_X) \quad \cdots\cdots(55)$$

Torsional influence number:

$$f_\theta = \frac{1}{GJ_p}\left(l - \frac{8\xi_\Theta Rb}{3l}\right) + \frac{2}{EJ_x}\left(R - \frac{2R^2\xi_\Theta}{3l}\right) \quad \cdots\cdots(56)$$

where $\xi_X = f_{X\Psi}/f_{\Psi\Psi}$, $\xi_\Theta = f_{\Theta\Phi}/f_{\Phi\Phi}$.

All symbols in formulae (55) and (56), $f_{X\Psi}$, $f_{\Psi\Psi}$, $f_{\Theta\Phi}$ and $f_{\Phi\Phi}$ have the same meanings as in Section 3.2.

Natural frequencies were calculated on HITAC 5020E, utilizing the same program as for the coupled vibration. They are compared with the solutions of coupled system in Table 13 and show little difference except the cases strongly coupled. Also the vibration modes scarcely differ, although the axial ones

Table 13. Comparison between calculated natural frequencies with and without coupling.

Ship	S				B	
Mode	Measured values	Without coupling $k_o=0.90\times10^7 kg/cm$	With coupling $k_o=0.90\times10^7 kg/cm$	Without cou. / With cou.	Measured values	Without coupling $k_o=0.20\times10^7 kg/cm$
1-node Tor.	V.P.M.	189.19	189.28	1.00		144.83
0-node Axi.	985	983.23	963.79	1.02	513	502.63
1-node Axi.	1064	1046.15	1034.46	1.01	765	739.00
2-node Tor.	1101	1050.50	1093.68	0.96	844	805.60
3-node Tor.		1681,46	1683.47	1.00		1303.86

	M				
With coupling $k_o=0.20\times10^7 kg/cm$	Without cou. / With cou.	Measured values	Without coupling $k_o=0.25\times10^7 kg/cm$	With coupling $k_o=0.25\times10^7 kg/cm$	Without cou. / With cou.
144.78	1.00	376	375.38	375.03	1.00
495.57	1.01	628	632.76	623.98	1.01
753.65	0.98		1367.36	1364.02	1.00
814.44	0.99	1005	1002.52	1015.18	0.99
1303.80	1.00		1898.38	1866.54	1.01

are different a little.

The computation was carried out in 4 seconds, giving 15 frequencies and normalized vibration modes succesively printed. About 4 seconds are also necessary for the same computer to solve 6 pairs of frequency and mode of an eight mass (6 cylinders, flywheel and propeller) system with conventional Holzer method, which necessitates in advance as many frequency approximations as required solutions.

6. Conclusions.

From the above analysis the following conclusions may be drawn :

(1) A new equivalent model of cranksfaf is contrived, which enables to analyze axial vibration, torsional vibration and two kinds of lateral vibrations without isolation from each other applying matrix technique.

(2) For this model system a method of solution is developed, utilizing the matrix technique and the digital computer. This method has revealed the coupled axial-torsional solution for the first time. Furthermore, every required frequency and mode are given at a time, though a rather bigger computer is necessary for a multi-cylinder engine shafting.

(3) Theoretical formulae to derive crank

stiffnesses from shaft dimensions are obtained and a method to estimate thrust block stiffness is proposed, combining measured frequency of nodeless mode with the equation of inertia force balance

(4) Eight cylinder semi-built, nine cylinder full-built and ten cylinder semi-built crankshaftings were analyzed with this new method and comparison between calculated results and measured ones show fairly excellent agreement. The results were also compared with those which were calculated with conventional Holzer method. Further, the effects of shaft dimensions were examined.

Their major results are as follows:

(1) The natural frequencies and corresponding mode shapes of torsional vibrations solved with the author's method are not so different from those usual Holzer solutions. Even in the case of strongly coupled axial-torsional vibration, the difference is not so great, but the usual method does not give the accompanied axial vibration mode.

2) The axial vibration mode, calculated with the usual method is different from the author's solution and the usual method can not give the uncoupled axial vibration mode.

3) Being the thrust block stiffness as small as the one of the independent block founded on the engine room floor, the stiffness strongly affects the axial vibration frequency depending on the mode shape of axial vibration. On the other hand, effect of thrust block stiffness on the torsional vibration is little except the case of strongly coupled vibration.

4) The arrangement of crank throw considerably affects the axial vibration but has only a little effect on the strongly coupled torsional vibration but has only a little effect on the strongly coupled torsional vibration. Therefore, the author proposes the firing order selection as a means to control the coupled axial vibration.

(5) The author's method also applies to uncoupled vibration analysis on digital computer more conveniently than the usual Holzer method.

7. Acknowledgement

The author wishes to express his thank to Prof. K. Tsuda for his kindly guidance and Dr. J. Hoshino, Dr. J. Arai and other staffs of Technical Research Laboratory, of Nippon Kaiji Kyokai for their helpfull suggestions and their kind supply of many worthwhile data.

References:

1) S. F. Dorey, Strength of marine engine shafting. Trans. N. E. C. Inst. Eng. and Shipb., Vol. 55, P. 203, 1938-39
2) P. Draminsky, et al., Axialschwingungen von Kurbelwellen. MTZ, H. 2, S. 49, 1942
3) R. Poole, The axial vibration of Diesel engine crankshaft. Proc. Inst. Mech. Eng., P. 167, 1941
4) J. R. Kane, et al., Longitudinal vibrations of marine propulsion-shafting systems. Trans. S. N. A. M. E., Vol. 58, P. 329, 1960
6) W. Benz, Die Erregung der Laengsschwingungen von Kurbelwellen, MTZ, H. 8, S. 333, 1960
7) G. Kern, Laengsschwingungen von Kurbelwellen grosser Schiffsdieselmotoren, MTZ, H. 2, S. 51, 1960
8) A. Guglielmotti, et al., Recheres experi-

mentales pour l'etude des vibrations axiales des vilebrequins. CIMAC, 1962, Copenhagen

9) G. Anderson, et al., Axial vibrations and measurements of stresses in crankshafts. Inter. Shipb. Progress, Vol. 10, No. 107, P. 235, 1963

10) A. J. Johnson, et al., Machinery induced vibrations. Trans. Inst. Marine Eng., Vol. 75, No. 4, P. 121, 1963

11) Van Dort, Crankshaft coupled free torsional axial vibrations of a ship's propulsion system. Inter. Shipb. Progress, Vol. 14, P. 333, 1963

12) A. Kleiner, Axial vibration of the crankshaft and propeller shafting of motorship, Inter. Shipb. Progress, Vol. 11, P. 36, 1964

13) N. J. Visser, and Van der Linden, The axial stiffness of marine Diesel engine crankshafts Part 1 and Part 2, Inter. Shipb. Progress, Vol. 14, P. 452 1967

14) A. Urshibara, et al., A theoretical consideration on the axial vibration of crankshaft, Nainen Kikan, Vol. 7, 1967 (in Japanese)

15) I. Endo. et al., The axial vibration of 2-cycle marine dissel engine shafting. Bulletine of Nippon Kaiji Kyokai, Nov. 1964, Nov. 1965, May 1967 (in Japanese)

16) R. E. D. Bishop, et al., The matrix analysis of vibration. Cambridge Press, 1965

17) E. C. Pestel, et al., The matrix analysis of vibration. Cambridge Press, 1965

18) P. Lancaster, Lambda-matrices and vibratory systems, Pergamon Press. 1966

19) K. Tsuda, Dynamics of machinery, Sankaido, 1957, (in Japanese)

20) T. Kato. Eigenvalue problem, Shokokushia, 1966 (in Japanese)

高出力 超音波發振器의 製作과 그의 特性

孫 珍 鉉

Construction and Characteristics of High Power Ultrasonic Generator

Jin Hyeon Son

Abstrat

A high power ultrasonic generator was constructed to improve the quality of fuel oil by means of ultrasonic treatment. This generator consists of the high frequency oscillater and the magnetostriction transducer made of nickel core.

The oscillator is operated at 30 kHz and its power is about 1, 8 kwatts.

This paper also presents the structure of the ultrasonic generator and measurement of its characteristice.

<目 次>

Ⅰ. 緖 論
Ⅱ. 裝置의 動作과 內容
Ⅲ. 測定結果
Ⅳ. 結 論

Ⅰ. 緖 論

本論文에서 製作한 超音波發振器는 "超音波照射에 依한 內燃機關用 低質油의 改善"에 關한 實驗用으로 製作한 것이다.

低質油改善에는 超音波의 cavitation 現象을 利用하는 것이므로 動力用으로써 cavitation이 容易하게 發生할 수 있어야 한다. 따라서 適合한 周波數와 持續的인 高出力의 超音波를 發生할수 있는 裝置가 要求된다.

여기서 製作한 超音波發振裝置는 周波數 30 kHz의 高周波出力 約 1.8 kw의 發振器와 超音波變換器로써 nickel core를 使用한 magnetostriction transducer로 構成되어 있다.

다음에서 이들 裝置의 構造와 特性의 測定値를 表示하였다.

Ⅱ. 裝置의 動作과 內容

本發振裝置는 그림 1의 回路圖와 그림 2의 全裝置圖와 같다.

그림 1에서 RC 發振器가 發振한 30 kHz의 高周波出力을 driving amp. 에서 增幅하고, 그의 出力은 L_1 C_1의 同調回路를 거쳐 並列로 接續한 高出力管 4-400A의 入力에 加해진다. 그리고 4-400A에서의 出力은 T_1에 供給된다. 이 T_1은 一次側 L_3와 C_{10}의 同調回路가 出力管의 最適負荷가 되고, 한편 二次側 L_4와 變換器가 impedance matching이 이루어지게 되어 있다. L_4에 誘起된 高周波電氣 energy는 超音波變換器의 coil에 供給되고, 한편 이 coil에는 bias用 直流電流